Journal of Inorganic Biochemistry 128 (2013) 1–10

Contents lists available at SciVerse ScienceDirect

Journal of Inorganic Biochemistry

journal homepage: www.elsevier.com/locate/jinorgbio

Inhibition of human prion neuropeptide PrP106-126 aggregation by hexacoordinated ruthenium complexes

Xuesong Wang, Bingbing Zhang, Cong Zhao, Yanli Wang, Lei He, Menghan Cui, Xiaotong Zhu, Weihong Du *

Department of Chemistry, Renmin University of China, Beijing 100872, China

ARTICLE INFO

Article history:
Received 8 March 2013
Received in revised form 5 July 2013
Accepted 8 July 2013
Available online 15 July 2013

Keywords:
Prion neuropeptide
Aggregation
Ruthenium complex
Inhibition
Ligand configuration

ABSTRACT

Prion disease is a neurodegenerative disorder that can occur among humans and other animals. The aberrant isoform of prion protein PrP^{Sc} has been identified as the infectious agent. The neuropeptide PrP106-126 has been widely used as a suitable model to study the biological and physiochemical properties of PrP^{Sc}. PrP106-126 shares several physicochemical and biological properties with PrP^{Sc}, including cellular toxicity, fibrillogenesis, and membrane-binding affinity. Ruthenium complexes are commonly employed in anti-cancer studies due to their low cellular toxicity. In this study, six hexacoordinated ruthenium complexes with different molecular configurations were used to investigate their effects on PrP106-126 aggregation inhibition. Results revealed that the interaction between the complexes and the peptide included metal coordination and hydrophobic interaction mainly. Those complexes with aromatic structure displayed better inhibitory effects, although they only had a common binding affinity to PrP106-126. This study provided better understanding on the interaction of metal complexes with PrP106-126 and paved the way for potential Ru-based metallodrugs against prion diseases.

1. Introduction

Prion diseases or transmissible spongiform encephalopathies (TSE) comprise a family of fatal neurodegenerative disorders. These diseases infect humans with the Creutzfeldt–Jakob disease (CJD), the Gerstmann–Sträussler–Scheinker syndrome (GSS), and Kuru, while other animals are infected with bovine spongiform encephalopathy (BSE), chronic wasting disease, and scrapie [1,2]. All these diseases have been associated with the accumulation of misfolding protein, which is an aberrant isoform of the prion protein (PrP^{C}) and is named as PrP^{Sc} [3,4]. PrP^{C} is a common membrane protein expressed in the entire body, predominantly in the central nervous system of mammalian species. However, the biological function of PrP^{C} is still unclear. Several experiments have suggested that PrP^{C} can bind metal ions in vivo, such as copper (Cu), zinc (Zn), and manganese (Mn), and is involved in the homeostasis of trace elements, enzymatic activity, and cellular signal transduction processes [5,6]. Earlier reports propose that this protein may represent an important tool in the treatment of cardiovascular diseases by angioplasty [7]. In vivo human and chicken PrPs exhibit SOD-like activity associated with octarepeat and hexarepeat regions. The fact that Cu (II) ion binds to hexapeptide repeat region of avian prion via side chain imidazoles of histidine residue reveals the highest SOD activity [8].

The abnormal scrapie isoform PrP^{Sc} has been considered as the infectious agent. PrP^{Sc} has an identical primary structure to PrP^{C}, but different secondary structure elements. PrP^{Sc} has significantly more β sheets and lesser α helix compared with PrP^{C} [9]. PrP^{C}–PrP^{Sc} conversion results in significant protein conformational change in their physicochemical properties, without any chemical modification.

PrP^{Sc} is resistant to protease K and shows a strong tendency toward aggregation into insoluble fibrils that disrupt neuronal function. The mechanism through which PrP^{Sc} catalyzes PrP^{C} from helical protein to β sheet-contained aggregates has not yet been elucidated, as well as the complete structure of PrP^{Sc}. The neuropeptide PrP106-126 (106-KTNMKHMAGAAA AGAVVGGLG-126), a N-terminal fragment of the human prion protein, has been widely used as a suitable model to study the biological and physiochemical properties of PrP^{Sc}. PrP106-126 is highly conserved among various species and has been suggested as the most important region to initiate conformational change and to lead the conversion of PrP^{C} to PrP^{Sc} [10–12]. PrP106-126 shares several physicochemical and biological properties with PrP^{Sc}, including cellular toxicity, fibrillogenesis, and membrane-binding affinity [13]. Furthermore, the toxicity of PrP^{Sc} and PrP106-126 requires the expression of PrP^{C} to cause cell death, and they can bind with PrP^{C} at 112–119 residues [14]. PrP106-126 is composed of two distinct regions, namely, the hydrophilic (K106-M112) and hydrophobic (A113-G126) regions. The toxicity of PrP106-126 has been assumed to be correlated with its primary sequence. Different synthetic and recombinant PrP-derived peptides (mainly PrP106-126), as far as mechanisms of aggregation and amyloid formation are concerned have been studied to reveal how these different spatial conformations affect neuronal death [15]. PrP106-126 shows a high tendency to aggregate into the β-sheet structure, forming amyloid fibrils in vitro and becoming partially

* Corresponding author. Tel./fax: +86 10 62512660/6444.
E-mail address: whdu@chem.ruc.edu.cn (W. Du).

0162-0134/$ – see front matter © 2013 Published by Elsevier Inc.
http://dx.doi.org/10.1016/j.jinorgbio.2013.07.009

resistant to proteolysis K [16,17]. Recent studies reported that the oligomerization of PrP106-126 emerged from the association of ordered-hairpin monomers rather than of disordered monomers [18,19]. Earlier-ordered oligomers were stacked by the interface of hydrophobic C-terminal residues (A113-G126), which may increase the rate of fibril growth and ultimately form the fibril structure [20]. Physical strategies for inhibiting amyloid fibril formation, including high hydrostatic pressure, low temperature, and laser irradiation, were critically evaluated [21]. Another work employed recombinant yeast-derived molecular chaperon Hsp104 to inhibit the fibril assembly of the synthetic PrP106-126 peptide. Hsp104 was able to disassemble the mature PrP106-126 fibrils in vitro, recovering the cytotoxicity of PrP106-126 on SK-N-SH cells [22].

The relationship between the amyloid structure and its peptide toxicity implies that PrP106-126 toxicity may be inhibited in case the amyloid structure failed to form. A number of studies demonstrated that divalent metal cation binding to PrP106-126 modulated its aggregation and neurotoxic properties, and the histidyl residue is crucial to bind metal cations [5,6,23–25]. Interestingly, recent studies found potential therapeutic applications of metal compounds for the treatment of Alzheimer's disease by targeting the metal binding site and by alkylating the imidazole side chains of Aβ [24,26]. In addition, our previous investigation on the interactions of Pt-, Pd-, and Au-based metal complexes with PrP106-126 demonstrated that tetra-coordinated complexes markedly affected the conformation of PrP106-126 and inhibited its aggregation by metal coordination, suggesting a new approach for the design and development of metallodrugs against prion diseases [27,28].

The well-developed synthetic chemistry of ruthenium (Ru), particularly with am(m)ine and imine ligands, provides several approaches to innovative metallopharmaceuticals [29]. Increasing knowledge on the biological effects and lower cellular toxicity of Ru complexes had been reported in the study of the fundamental characteristics of Ru complexes on drug developments [30–32]. Ru complexes using am(m)ine as ligands selectively bind to imine sites, such as histidyl imidazole nitrogens on proteins and the N7 site on the imidazole ring of purine nucleotides [29]. The role of Ru-based compounds in the interaction with Aβ amyloid protein has also been previously reported [33,34]. In the present study, a series of hexacoordinated Ru complexes (Scheme 1) have been synthesized, aiming to elucidate their interactions with PrP106-126. In addition, changes in the physicochemical properties of PrP106-126 induced by different Ru complexes are observed and the relationship between the ligand property and aggregation of this active peptide is clarified, for the development of novel therapeutic agents against prion diseases.

2. Materials and methods

2.1. Materials

Human prion protein fragment PrP106-126 was chemically synthesized by the SBS Co. Ltd. (Beijing, China) and further purified and identified by HPLC and mass spectrometry (MS) with more than 95% purity. The peptide in this study had free C and N termini, unless otherwise specified. The Ru complexes were prepared as described in literature [35–41]. The Ru complexes were dissolved in DMSO or d6-DMSO and stored at −20 °C for future use. All other reagents were of analytical grade.

2.2. Electrospray ionization mass spectrometry (ESI-MS)

The peptide concentration used in MS determination was constant at 50 μM. Equivalent Ru complex was incubated with the peptide. ESI-MS spectra were recorded in the positive mode via direct introduction of the samples at 3 $\mu L \cdot min^{-1}$ flow rate using an APEX IV FT-ICR high-resolution mass spectrometer (Bruker, USA), equipped with a conventional ESI source. The working condition included the following: end plate electrode voltage, −3500 V, capillary entrance voltages, −4000 V, skimmer 1 voltage, 30 V, and 200 °C dry gas temperature. The flow rates of the drying and nebulizer gases were set at 12 and 6 $L \cdot min^{-1}$, respectively. The Data Analysis 4.0 software program (Bruker) was used for acquisition, and the deconvoluted masses were obtained using the integrated deconvolution tool.

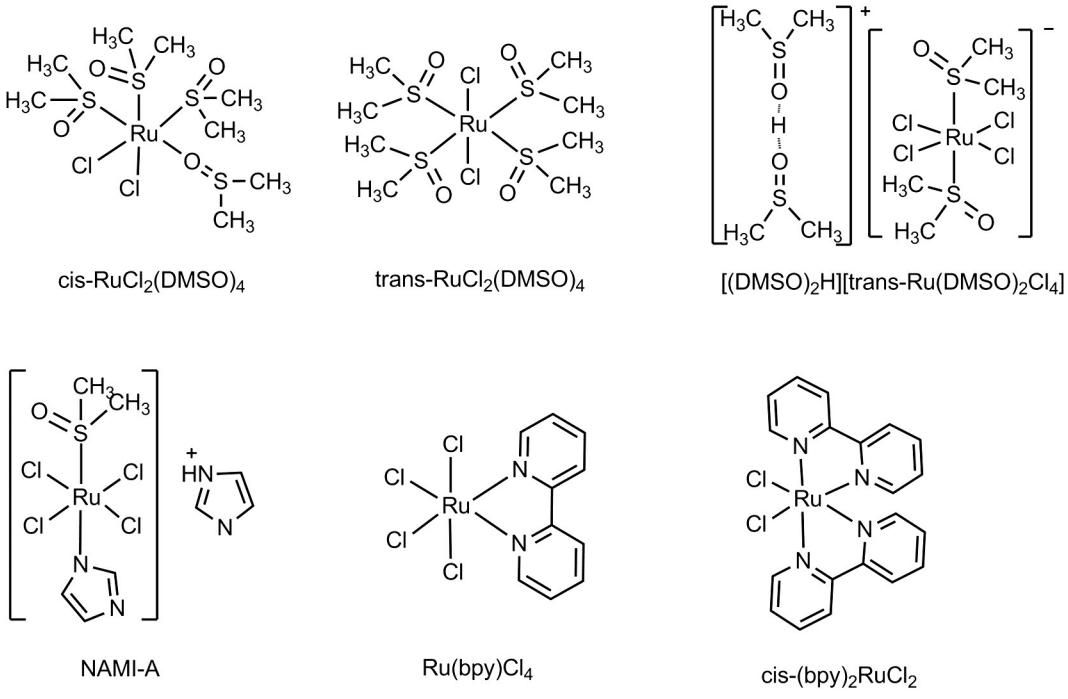

Scheme 1. Molecular structure of hexacoordinated Ru-complexes.

2.3. NMR experiments

The ^1H–^1H TOCSY (total correlation spectroscopy) experiments were carried out to identify the probable binding site between ruthenium complex and PrP106-126. Here the complexes NAMI-A ([trans-$RuCl_4$(DMSO)(Im)][ImH]) and cis-$(bpy)_2RuCl_2$ (bpy: bipyridine) were selected as the model. The final concentration of the peptide was 1 mM, and double amounts of complex were added to the peptide solution. The sample for NMR study was prepared in H_2O containing 10% d6-DMSO. The 2D NMR experiments were performed on a Bruker Avance 600 MHz spectrometer at 25 °C. Suppression of the residual water signal was achieved by the WATERGATE pulse program with gradients.

2.4. Circular dichroism spectroscopy

Circular dichroism (CD) spectra were obtained through a Jasco J-810 spectropolarimeter (Japan Spectroscopy Co., Japan). The sample was prepared in 5 mM phosphate buffer at pH 7.2. The final peptide concentration was 0.1 mM. A 1 mm quartz cell was used for all CD spectra. The spectra were recorded between 190 and 250 nm with 0.5 nm spectral step and 2 nm bandwidth. A scan rate of 100 nm min^{-1} with 1 s response time was employed. The background spectrum of corresponding Ru-complex was removed using the same buffer. The final spectrum for each sample was derived from the average of three repeated experiments.

2.5. Thioflavin T (ThT) assay

After the solution of 0.1 mM PrP106-126 at 10 mM phosphate buffer at pH 7.2 was aged, equivalent Ru complex was added and the sample was incubated with 10 μM ThT, and sample fluorescence was monitored using an LS55 spectrofluorometer (PerkinElmer, USA). The ThT signal was quantitatively measured by averaging the fluorescence emission at approximately 500 nm for over 10 s, when excited at 432 nm. The final spectrum was obtained from the mean of three repeated spectra. In consideration of possible inner filter effect of Ru-complexes, ThT fluorescence spectrum was carried out after addition of aromatic-ring containing Ru-complexes.

For the IC50 determination, the concentrations of Ru complexes were selected at 0 μM, 20 μM, 40 μM, 60 μM, 100 μM and 200 μM respectively.

2.6. Transmission electron microscopy (TEM)

Samples were prepared by mixing equivalent Ru complex with 5 mM peptide solution, and then incubated at 37 °C for 24 h. The final peptide concentration used in the TEM experiment was 0.1 mM, with 1% DMSO. An aliquot of each sample was spotted onto carbon-coated 600-mesh copper grid and was negatively stained by 2% phosphotungstic acid. Air-dried specimens were examined and photographed using a Hitachi H-800 electron microscope (Hitachi, Japan) at 200 kV. The final photo used was from the mean of three repeated data.

2.7. Atomic force microscopy (AFM)

Samples were prepared by mixing equivalent Ru complex with 5 mM peptide solution, and then incubated at 37 °C for 24 h. The final peptide concentration used in the AFM experiment was 0.1 mM, with 1% DMSO. Images were obtained in the tapping mode with a silicon tip under ambient conditions, a scanning rate of 1 Hz, and a scanning line of 512 using the Veeco D3100 instrument (Veeco Instruments 151 Inc., USA).

3. Results

3.1. Synthesis of the ruthenium complexes

Synthesis of cis-$RuCl_2(DMSO)_4$ was completed according to the earlier literatures [35,36]: 78 mg $RuCl_3 \cdot 3H_2O$ was dissolved in 2.1 mL DMSO and hydrogen was bubbled through at 80 °C for 10 h. The yellow crystalline material was collected and washed with benzene and dried under nitrogen (yield 88%). Recrystallization was performed from benzene–DMSO solution. The complexes with DMSO ligand have only simple and undistinguished NMR signal, so the infrared spectroscopy (IR) was employed to confirm its identity. The IR spectral bands of cis-$RuCl_2(DMSO)_4$, observed at 351 cm^{-1}, 383 cm^{-1}, 424 cm^{-1}, 482 cm^{-1}, 677 cm^{-1}, 717 cm^{-1}, 937 cm^{-1}, 960 cm^{-1}, 993 cm^{-1}, 1024 cm^{-1}, 1097 cm^{-1}, 1114 cm^{-1}, 1290 cm^{-1}, 1309 cm^{-1}, 1400 cm^{-1}, and 1419 cm^{-1}, corresponded with the reported literature [35].

Synthesis of trans-$RuCl_2(DMSO)_4$ was carried out referring to earlier report [37]: Recrystallized cis-$RuCl_2(DMSO)_4$ (50 mg) was dissolved in 4 mL of DMSO by gentle heating at 80 °C. The solution was transferred into a water-cooled photoreactor equipped with a 125-W lamp and irradiated for 4 h. During the reaction, the solution temperature was kept close to room temperature. The whole procedure was conducted under an inert gas atmosphere. The yield was 80%. Similarly, characteristic IR bands at 1080 cm^{-1} and 416 cm^{-1} of the complex trans-$RuCl_2(DMSO)_4$ were also detected.

Synthesis of the complex $[(DMSO)_2H][trans\text{-}Ru(DMSO)_2Cl_2]$ [38]: The amount of 100 mg $RuCl_3 \cdot 3H_2O$ was refluxed in 10 mL of ethanol for 3 h. The deep green solution was then filtered and vacuum-evaporated to the volume of 1 mL. A 0.1 mL of 37% aqueous HCl and 0.2 mL of DMSO were added, and the solution was heated to 80 °C under stirring. Within 10 min its color turned to red-orange. 2 mL of acetone was added to the cooled transparent solution. The formed red crystals were filtered off, washed with cold acetone and diethyl ether, and vacuum-dried (yield 70%). The complex was also confirmed using IR spectrometry. The bands at 345 cm^{-1}, 416 cm^{-1}, 968 cm^{-1}, 1016 cm^{-1}, 1112 cm^{-1}, 1290 cm^{-1}, 1301 cm^{-1} and 1398 cm^{-1} were verified.

Synthesis of NAMI-A [39]: 100 mg $[(DMSO)_2H][trans\text{-}Ru(DMSO)_2Cl_4]$ was dissolved in 2 mL of acetone and then stirred for 4 h after the addition of 49 mg imidazole. The deposit turned into brick red from orange. After filtration, the product was washed with acetone and diethyl ether and vacuum-dried (yield 90%).

Synthesis of $Ru(bpy)Cl_2$ [40]: 86 mg $RuCl_3 \cdot 3H_2O$, 60 mg KCl and 93.6 mg 2,2′-bipyridine were dissolved in 5 mL of 1 M HCl and stirred at 30 °C for 72 h. The deposit was filtered and washed with acetone and diethyl ether, and vacuum-dried. The product was suspended in 5 mL of 0.2 M HCl and bubbled with Cl_2 for 15 min, and then stirred for 1 h. After filtration, the almost black solid was washed with ice-water and dried in a vacuum (yield 56%).

Synthesis of cis-$(bpy)_2RuCl_2$ [41]: 78 mg commercial $RuC1_3 \cdot 3H_2O$, 93.6 mg 2,2′-bipyridine and 84 mg LiCl were heated together at reflux in 5 mL of DMSO for 8 h. After the reaction mixture was cooled to room temperature, 5 mL of acetone was added and the resultant solution was cooled at 0 °C overnight. Filtering the yielded red to red–violet solution, a dark green–black microcrystalline was produced. The solid was washed three times with water followed by diethyl ether, and then it was dried by suction (yield 76%).

The aromatic-ring containing ruthenium complexes were confirmed by NMR experiment and the ^1H NMR spectra were shown in Fig. S1.

3.2. ESI-MS study on the binding of Ru complexes to PrP106-126

Duple amounts of Ru complexes were incubated with the peptide PrP106-126, and then the final solution was analyzed by ESI-MS to determine whether Ru complexes directly bind to PrP106-126. The

resulting ESI-MS deconvoluted spectra are shown in Figs. 1 and 2. Free PrP106-126 exhibited an intense peak at 1911.99 Da (1+), corresponding to its expected mass (Fig. 1A). The spectra appeared different after various Ru complexes were incubated with PrP106-126. Fig. 1B and C illustrated the mass spectrum of PrP106-126 after incubation with cis-$RuCl_2(DMSO)_4$ and trans-$RuCl_2(DMSO)_4$. The peak at 2160.84 Da was referred to the adduct of [PrP106-126 + $RuCl_2(DMSO)$] (Fig. 1B), whereas the m/z value of 1121.44 Da (2+) was assigned to the adduct of [PrP106-126 + $RuCl_2(DMSO)_2$] (Fig. 1C). Fig. 1D demonstrated that the treatment of peptide with [$(DMSO)_2H$][trans-$Ru(DMSO)_2Cl_4$] led to the emergence of additional peaks at 2153.77, 2231.78, and 2553.57 Da (1+), which were directly assigned to the metal–peptide adducts. The increase in mass of 241, 319, and 641 Da matched the fragments of $RuCl_4^-$, $RuCl_4(DMSO)^-$, and 2[$RuCl_4(DMSO)^-$], respectively. This result suggested that the compounds bound to PrP106-126 at 1:1 and 2:1 ratios with one or two displaced DMSO ligands due to hydrolysis of the compound in aqueous solution.

The incubation of NAMI-A with PrP106-126 (Fig. 2B) produced a different spectrum with new intensity peaks at 1151.92 and 1347.33 (2+). These results indicated that NAMI-A was bound to the peptide at 1:1 and 2:1 ratios in the form of [Ru(DMSO)(Im)Cl_4], which denoted that the outside Him^+ group in NAMI-A slipped off during the adduct formation. The new peak at 2317.91 Da (1+) for the treatment of Ru(bpy)Cl_4 with PrP106-126 was referred to the adduct of [PrP106-126 + Ru(bpy)(DMSO)Cl_2] (Fig. 2C). The new adduct may contribute to the hydrolysis of Ru(bpy)Cl_4. The mass spectrum from the incubation of cis-$(bpy)_2RuCl_2$ with PrP106-126 (Fig. 2D) showed two obvious peaks assigned to the adducts of [PrP106-126 + Ru] (2009.94 Da) and [PrP106-126 + Ru(bpy)Cl_2] (2243.15 Da). The ESI-MS results revealed that Ru complexes could bind to PrP106-126 in different binding modes. A table was given to show all the detected m/z values and the estimated data of all adducts (Table S1). The difference between the detected data and estimated data may be attributed to the dissociation of the hydrogen.

3.3. The probable binding sites between PrP106-126 and Ru complexes

2D NMR method was used to identify the possible binding site of Ru Complex with PrP106-126. Here the complexes NAMI-A and cis-$(bpy)_2RuCl_2$ were selected as the model. Fig. 3 compared the ^1H–^1H TOCSY spectra recorded with or without 2.0 equiv of NAMI-A. The C_δHs, NH of the His111 and C_βHs, C_γHs, and NH of Met112 showed chemical shift change and weaker intensity due to peak relaxation. Other spin system such as Lys110 was also slightly affected (Fig. S2). Due to the appearance of [Ru(DMSO)(Im)Cl_4] in ESI-MS spectrum, hydrophobic interaction but not direct metal coordination was assumed for the binding of NAMI-A with PrP106-126. The possible binding site was from Lys110, His111 and Met112. In addition, the cis-$(bpy)_2RuCl_2$ complex did not change the methionine spin system but the C_δHs of His111 as shown by peak broadening and chemical shift change (Fig. S3). Moreover, the spin system of Lys110 was not disturbed by the complex cis-$(bpy)_2RuCl_2$ (Fig. S4). Since the product of Ru(bpy)Cl_2 was observed in ESI-MS, free metal binding site was remained to the peptide. And the most possible metal binding site was His111 for the interaction of cis-$(bpy)_2RuCl_2$ and PrP106-126.

3.4. PrP106-126 conformational changes induced by Ru complexes

Circular dichroism (CD) spectroscopy was employed to examine the effect of Ru complexes on the conformation of PrP106-126 at physiological pH. The peptide in a 5 mM phosphate buffer at pH 7.2 exhibited a predominately negative CD absorbance at 197 nm as the typical random coil structure. Negative ellipticities were also revealed in the 210 nm to 230 nm region, suggesting that the peptide was characterized by the presence of small amounts of secondary structural elements. The addition of equivalent Ru complexes induced the disturbance of the negative CD absorbance at 197 nm (Fig. 4). Cis-$RuCl_2(DMSO)_4$ and [$(DMSO)_2H$][trans-$Ru(DMSO)_2Cl_4$] displayed

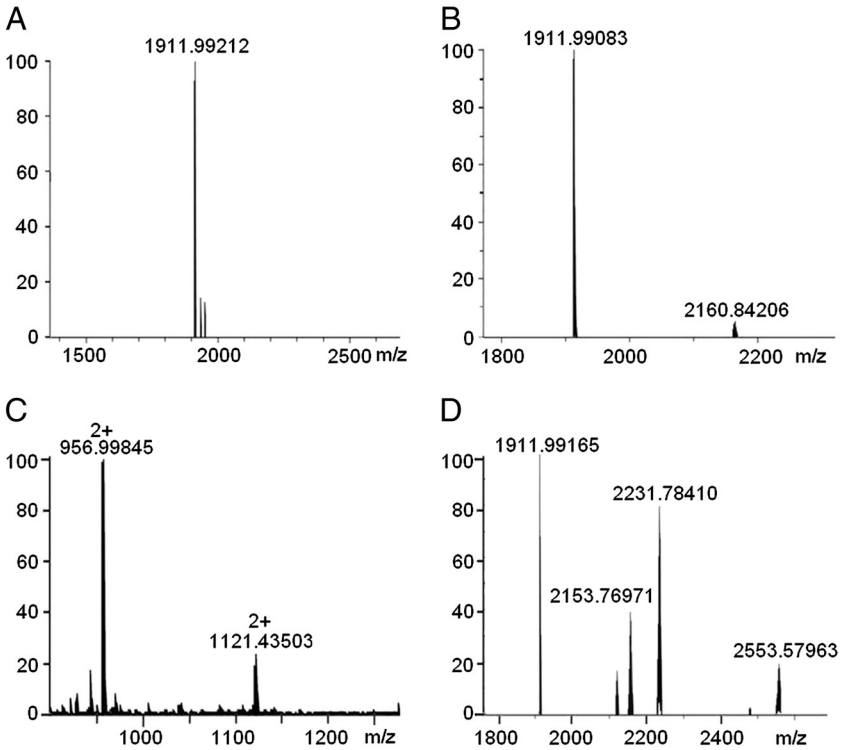

Fig. 1. Deconvoluted ESI-MS spectra of PrP106-126 in the absence (A) and presence of cis-$RuCl_2(DMSO)_4$ (B), trans-$RuCl_2(DMSO)_4$ (C), and [$(DMSO)_2H$][trans-$Ru(DMSO)_2Cl_4$] (D). The aqueous mixture was prepared by adding double amounts of Ru complexes to PrP106-126. The solution was diluted in water to a final concentration of 50 μM.

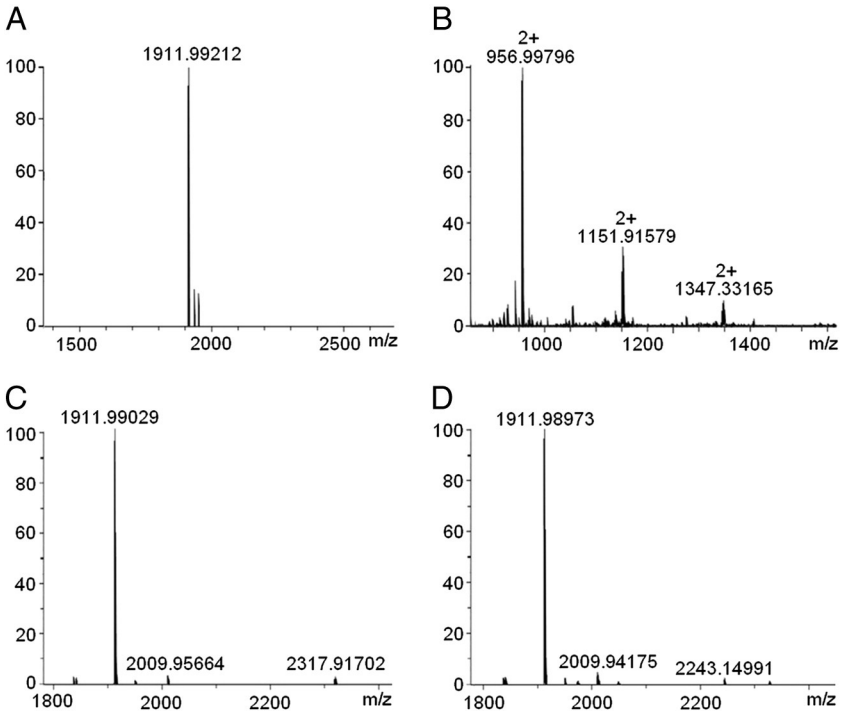

Fig. 2. Deconvoluted ESI-MS spectra of PrP106-126 in the absence (A) and presence NAMI-A (B), $Ru(bpy)Cl_4$ (C), and cis-$(bpy)_2RuCl_2$ (D). The aqueous mixture was prepared by adding double amounts of Ru complexes to PrP106-126. The solution was diluted in water to a final concentration of 50 μM.

the most effective change in the spectra. The difference is that cis-$RuCl_2(DMSO)_4$ decreased the absorbance at 197 nm, whereas $[(DMSO)_2H][trans\text{-}Ru(DMSO)_2Cl_4]$ increased the absorbance. In addition, the complex trans-$Ru(DMSO)_4Cl_2$ and NAMI-A did not obviously change the peptide conformation. The change in the CD spectra of PrP106-126 with $Ru(bpy)Cl_4$/cis-$(bpy)_2RuC1_2$ was similar to

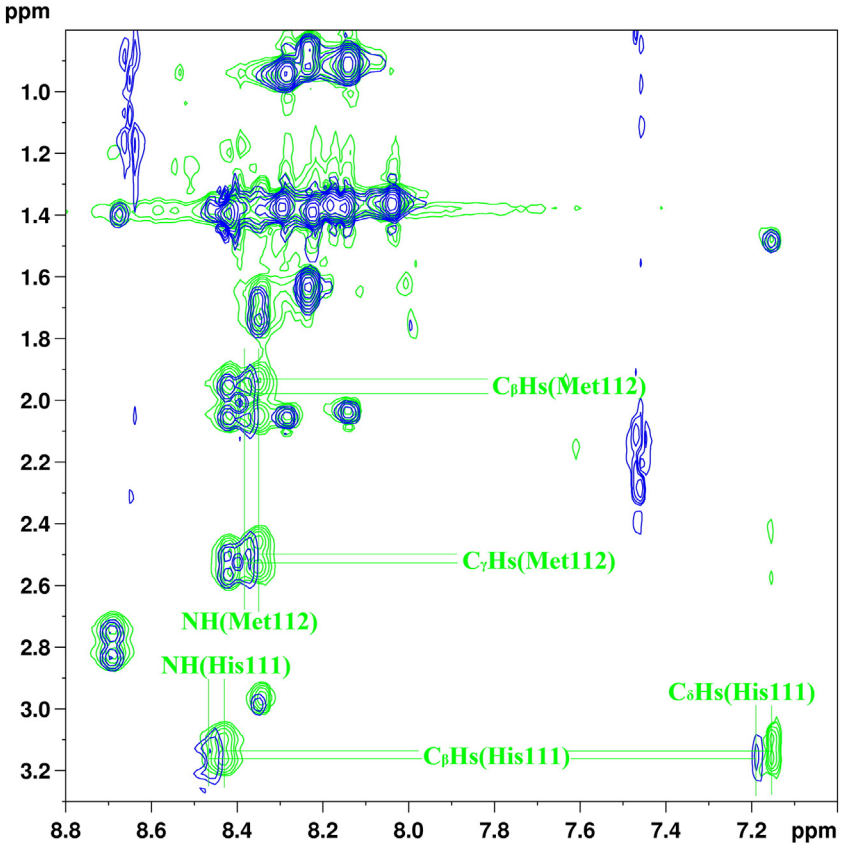

Fig. 3. Portion of ^1H–^1H TOCSY spectrum of 1 mM PrP106-126 at pH 5.7 and 25 °C in the absence (light green) and presence (dark blue) of 2.0 equiv of NAMI-A. (For interpretation of the references to color in this figure legend, the reader is referred to the web version of this article.)

that of $[(DMSO)_2H][trans\text{-}Ru(DMSO)_2Cl_4]$, which indicated the influence of metal complexes on PrP106-126 conformation (Fig. S5).

3.5. ThT analysis of PrP106-126 aggregation induced by Ru complexes

The neuropeptide PrP106-126 is essential to the aggregation of PrP^{Sc}, which is correlated with prion protein toxicity. The aggregation of PrP106-126 can be monitored by ThT assay that results in a new excitation at 432 nm and enhanced emission around 500 nm. Fig. 5 shows that the spectrum presented a strong fluorescence signal when ThT was bound to PrP106-126. However, ThT fluorescence significantly decreased after the incubation of PrP106-126 with Ru complexes for 24 h, suggesting that the formation of the fibril structure was effectively inhibited. Interestingly, $cis\text{-}(bpy)_2RuCl_2$ and $Ru(bpy)Cl_4$ complexes exhibited stronger inhibition effects on the aggregation of PrP106-126 after the incubation of PrP106-126 with Ru complexes for 10 h, whereas other complexes exhibited generic fluorescence quenching to the peptide (Fig. S6). In consideration of the inner filter effect, the ThT fluorescence intensity was disturbed a little bit by the aromatic-ring containing Ru-complexes (Fig. S7), but the disturbance was negligible compared with strong fluorescence decrease after the incubation of PrP106-126 with the aromatic-ring containing Ru-complexes. The concentration-dependent inhibitive effects of different ruthenium complexes on PrP106-126 aggregation analyzed by ThT fluorescence are shown in Fig. S8. Table 1 shows the IC50 value for different Ru complexes, and $Ru(bpy)Cl_4$ displayed the most effective inhibition with its IC50 at 6 μM.

3.6. PrP106-126 aggregation images by TEM and AFM

TEM and AFM were performed to ascertain whether Ru complexes affect peptide aggregation and fibril formation. The aggregates formed by PrP106-126 displayed a quasi-spherical structure (Fig. 6A), which potentially implies a strong aggregation state, after 24 h of incubation at 37 °C [27,28]. However, the TEM and AFM micrographs of PrP106-126 in the presence of Ru complexes showed that the aggregation was reversed to different extents. The morphology revealed a distinct shape after the incubation of Ru complexes with the aggregates for 24 h.

NAMI-A influenced the aggregates of PrP106-126 more effectively than that of $[(DMSO)_2H][trans\text{-}Ru(DMSO)_2Cl_4]$ (Fig. 7). Negatively stained fibrils, in the presence of $cis\text{-}RuCl_2(DMSO)_4$ and $trans\text{-}RuCl_2(DMSO)_4$, were branched and weaker than those of PrP106-126 (Fig. 6). The fibrils for $cis\text{-}(bpy)_2RuCl_2$ and $Ru(bpy)Cl_4$ were sparsely scattered, which indicated the more intense inhibiting ability of aromatic ring-containing complexes (Fig. 8).

Table 1
The IC50 value for the inhibition of ruthenium complexes on PrP106-126 aggregation measured with ThT fluorescence.

Ruthenium complex	Inhibition of fibril formation IC50 (μM)
$Cis\text{-}RuCl_2(DMSO)_4$	81
$Trans\text{-}RuCl_2(DMSO)_4$	22
$[(DMSO)_2H][trans\text{-}Ru(DMSO)_2Cl_4]$	8
NAMI-A	10
$Ru(bpy)Cl_4$	6
$Cis\text{-}(bpy)_2RuCl_2$	7

4. Discussion

PrP106-126 maintains the amyloidogenic and neurotoxic properties of the entire pathological PrP^{Sc} and is usually used as an acceptable model to study the mechanism of prion diseases [13]. Our previous study demonstrated that Pt-, Pd- and Au-based complexes altered the solution properties of PrP106-126 and significantly inhibited prion fragment aggregation [27,28]. However, the molecular configuration of selected compounds in the abovementioned types of complexes is limited. In this study, hexacoordinated Ru complexes were employed in view of varied ligand configurations to study their inhibition abilities to PrP106-126.

4.1. Different binding modes of Ru complexes to PrP106-126

Ru-based complexes can reportedly bind to several peptide fragments or proteins [42,43]. In this study, six hexacoordinated Ru complexes were used to bind the prion neuropeptide PrP106-126 and change the physicochemical properties of PrP106-126. In the ESI-MS experiments, Ru complexes were used to interact with the peptide after diluting the stock solution. Many other reports proposed the hydrolysis property of ruthenium complexes [29,44]. In this study, some compounds suffered the process, yet they bound to PrP106-126 at lower concentration (see ESI-MS data for different products), which indicates that the complexes have better binding affinity to PrP106-126. The ESI-MS spectra demonstrated that Ru complexes can interact with PrP106-126 in different binding modes as well. The $[(DMSO)_2H][trans\text{-}Ru(DMSO)_2Cl_4]$ compound bound with PrP106-126 at 1:1 and 1:2 ratios with one or two detached DMSO ligands. The formation of three adducts is presumably due to the solvolysis of the complex. NAMI-A has demonstrated its anti-metastatic activity in pre-clinical studies [35]. It can bind to surface histidyl imidazoles on albumin in the blood as NAMI [42,43]. In our study, NAMI-A bound to PrP106-126 at 1:1 and 2:1 ratios, with the release of the outer imidazole ring. The MS

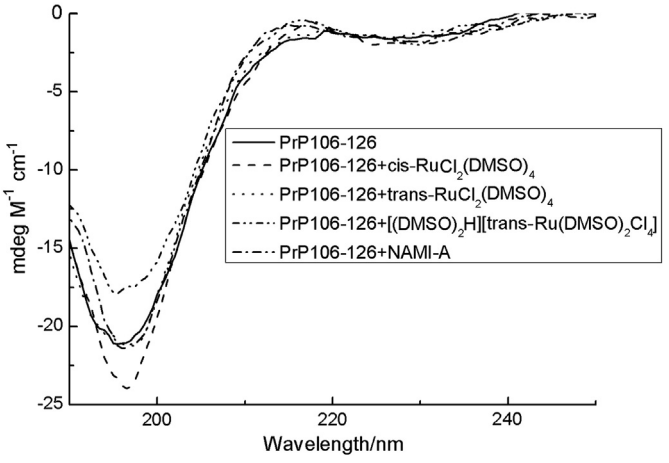

Fig. 4. Circular dichroism spectrum of PrP106-126 in the presence and absence (black line) of 1.0 equiv of ruthenium complexes. The PrP106-126 concentration in solution was 0.1 mM.

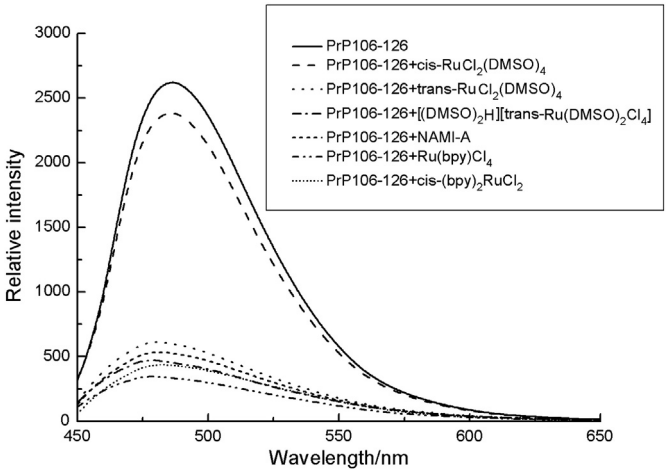

Fig. 5. Evaluation of the ability of the ruthenium complexes to inhibit PrP106-126 aggregation as measured by ThT fluorescence.

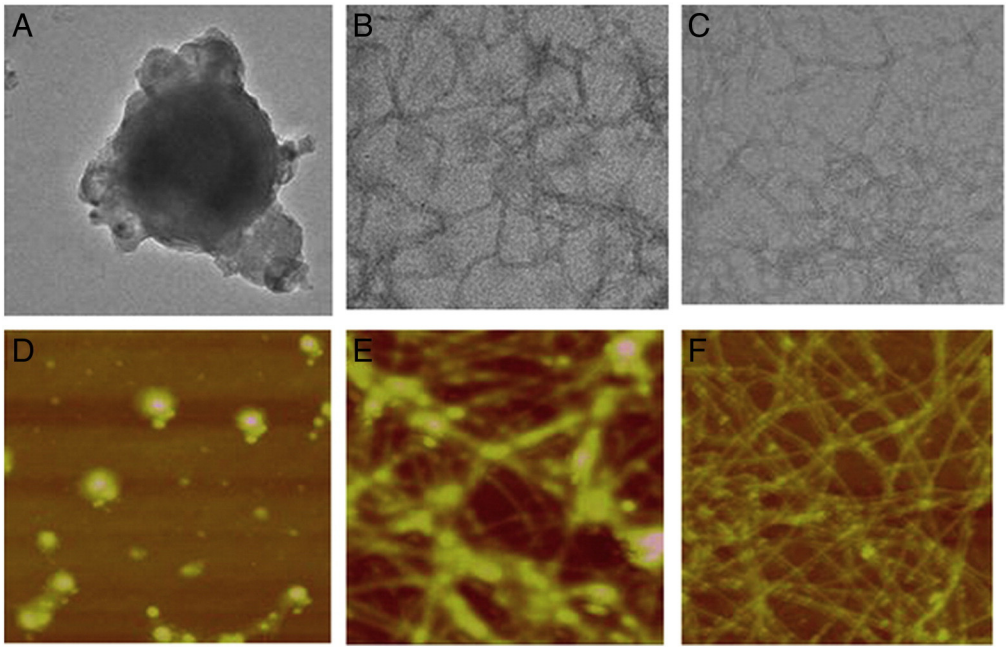

Fig. 6. TEM and AFM images of PrP106-126 fibrils in the absence (A, D) and presence of cis-$RuCl_2(DMSO)_4$ (B, E), and trans-$RuCl_2(DMSO)_4$ (C, F). The scale bar is 200 nm for TEM, and 1.5 μm for AFM.

data illustrated the absence of free metal binding site for NAMI-A binding to PrP106-126. This interesting phenomenon displayed a distinctive binding pattern from that of other ruthenium complexes. May non-bonded interactions such as hydrophobic interaction and electrostatic interaction contribute to the binding force between NAMI-A and the peptide. After binding with the compound, 2D ^1H–^1H TOCSY assay showed the resonance disturbance from His111, Met112, as well as Lys110. Moreover, the imidazole ring of His111 may play a π–π interaction role and the polar side chain of Lys110 may contribute to the electrostatic interaction.

In addition, MS spectra indicated that cis-$(bpy)_2RuCl_2$ and $Ru(bpy)Cl_4$ compounds bound to the peptide in two forms, e.g., only the Ru ion and relevant fractional group bound to the peptide. A common point of the two complexes is that the adduct scaffold of the peptide–metal complex reserved the aromatic ring. For the linear configuration of Ru complexes, cis-$RuCl_2(DMSO)_4$ and trans-$RuCl_2(DMSO)_4$ bound to PrP106-126 in different ways with varied numbers of DMSO ligand that slipped off. Comparing the relative peak intensities in the MS spectra, $[(DMSO)_2H][trans\text{-}Ru(DMSO)_2Cl_4]$ showed the strongest binding affinity among the studied complexes. This strong binding affinity reveals that the conformation of the complexes contributed to the binding affinity with the peptide.

The ^1H–^1H TOCSY spectrum demonstrated a probable binding mode between Ru complex and PrP106-126. NAMI-A binds to the peptide through non-bonded interaction, because the product $[Ru(DMSO)(Im)Cl_4]$ from ESI-MS shows no direct metal coordination to the peptide. The 2D NMR results displayed that the spin system of Lys110, His111,

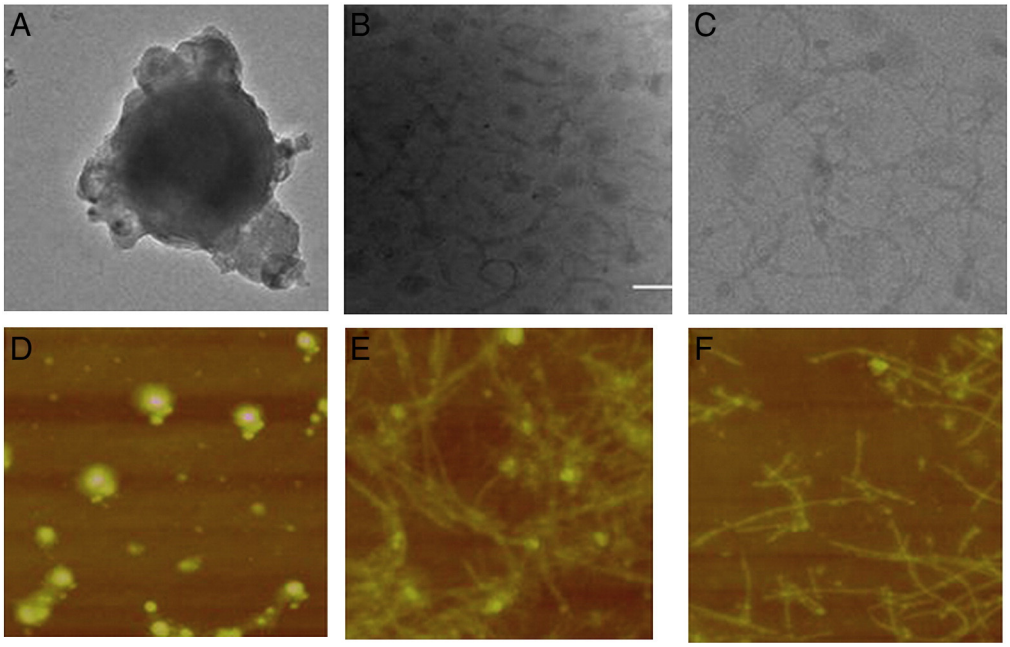

Fig. 7. TEM and AFM images of PrP106-126 fibrils in the absence (A, D) and presence of $[(DMSO)_2H][trans\text{-}Ru(DMSO)_2Cl_4]$ (B, E), and NAMI-A (C, F). The scale bar is 200 nm for TEM, and 1.5 μm for AFM.

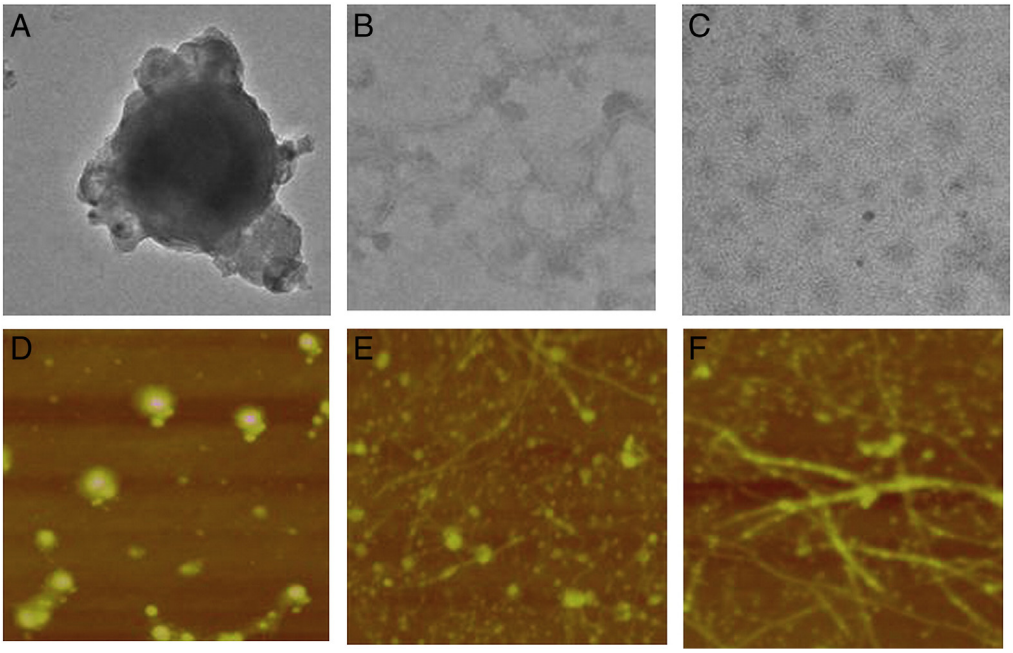

Fig. 8. TEM and AFM images of PrP106-126 fibrils in the absence (A, D) and presence of cis-$(bpy)_2RuCl_2$ (B, E), and $Ru(bpy)Cl_4$ (C, F). The scale bar is 200 nm for TEM, and 1.5 μm for AFM.

and Met112 was disturbed either in the peak shape or in the chemical shift. A presumption was made that the imidazole ring of complex NAMI-A interacts with the peptide at the N-terminal region, causing the change of the peptide biophysical properties. When it comes to the complex cis-$(bpy)_2RuCl_2$, only the chemical shift change of His111 $C_\delta Hs$ was observed, indicating the probable metal binding site to the peptide according to the ESI-MS result.

Different binding modes were also reflected by the CD spectra. The coordination of Ru complexes to PrP106-126 changed the secondary structure of the peptide at different degrees. Our conformational study revealed that cis-$RuCl_2(DMSO)_4$ induced an opposite effect on the conformation of PrP106-126, unlike other complexes. This opposite effect may be a result of the different binding modes of this complex with PrP106-126. Furthermore, the influence of trans-$RuCl_2(DMSO)_4$ and NAMI-A on the conformation of PrP106-126 was not obvious. However, the binding of the two compounds with PrP106-126 is solid from ESI-MS. Even though notable conformational change is not observed, the inhibitory effects of the two compounds on peptide aggregation are evident. This indicates no direct relationship between the binding mode and the inhibition of peptide aggregation for the two compounds. Maybe they affect some factors relative to fibril formation but not visible secondary structure change, such as spatial obstacle and β-sheet orientation.

4.2. Effective inhibition of Ru complexes on PrP106-126 aggregation

The binding interactions of Ru complexes with PrP106-126 were well identified by ESI-MS spectra. In addition, Ru complexes significantly affected the formation of the amyloid structures of PrP106-126 through ThT assay. Although minor inner filter effect did exist in the ThT assay, especially to those aromatic compounds, the main results were not impacted. Further, several earlier studies have employed the ThT assay to assess the effect of inhibitors on the fibril formation of Aβ protein [45–48]. And the IC50 values were also determined to compare the inhibition of different ruthenium complexes on preformed PrP106-126 fibrils. The IC50 results revealed that aromatic-ring containing complexes such as NAMI-A, $Ru(bpy)Cl_4$, and cis-$(bpy)_2RuCl_2$ exerted a stronger inhibitive effect on the fibrils formation. Compared with metal inhibitors of Aβ protein, the mentioned compounds have a better IC50 value under 10 μM [47]. All the results corresponded to the observed AFM and TEM images.

The peptide aggregation resulted from Ru complexes were also confirmed by TEM and AFM images, in which method no ThT binding competition was worried. The morphology of the aggregates formed by the prion peptide after incubation for 24 h is large in scale and volume. However, after treating with the Ru complexes, the aggregated neuropeptide changed into scattered and filamentous aggregates. All Ru complexes reversed the aggregation behavior of PrP106-126, despite varied inhibitory effects for different complexes. NAMI-A displayed a better inhibitory ability than that of $[(DMSO)_2H][trans\text{-}Ru(DMSO)_2Cl_4]$. The only difference between the two complexes was their ligands. NAMI-A bound to PrP106-126 in the form of [Ru(DMSO)(Im)Cl]. The adduct formed by PrP106-126 and NAMI-A reserved the aromatic ring imidazole, which may enlighten us with the proposal that the aromatic ring interacts with the peptide side chain such as imidazole group of His111. Ultimately, the conformation of aggregated peptide was affected and simultaneously the change of morphology of aggregates.

Former research proposed that the protofibril was an inevitable step during the process of aging fibrous peptides such as Aβ and prion peptides [49,50]. The observed protofibril after treating aggregated prion peptides with NAMI-A indicated that the complex reversed the fibrous state of PrP106-126. It has also been reported that oligomers formed by prion peptides or Aβ peptides maintained the structure of spherical like aggregates that can be detected under AFM or TEM instruments [51]. Although the morphology of aggregates was changed after treating cis-$(bpy)_2RuCl_2$ and $Ru(bpy)Cl_4$ with the aggregated fibril, clearance of the oligomers still needs further efforts.

However, cis-$(bpy)_2RuCl_2$ and $Ru(bpy)Cl_4$ demonstrated better inhibitory effects than that of cis- and trans-$RuCl_2(DMSO)_4$, which may be consequent to their aromatic pyridine ligand. Hence, potential π–π interaction between the aromatic compounds and PrP106-126 is supposed, aside from metal coordination and hydrophobic interaction. The aggregates may be composed of monomers, oligomers and fibrils. Particularly, the oligomers are cytotoxic. Therefore, more Ru compounds need to be studied for better deconstruction of oligomers and elimination of fibrils.

4.3. Comparison of Ru complexes binding affinity with inhibitory effect on PrP106-126

The MS spectra commonly display several adducts after the incubation of the complexes with PrP106-126. Interestingly, the Ru complexes, except for NAMI-A, bound to PrP106-126 in the metal coordination mode because Ru ion-contained fragment was always observed in the MS spectra of the peptide-complex mixing solution. The MS data suggested that the binding affinity of Ru complexes is not better than that of Pd complexes [28], whereas the inhibitory effect of ad hoc complexes is greater in NAMI-A, $Ru(bpy)Cl_4$, and $cis\text{-}(bpy)_2RuCl_2$. The MS data collected after the incubation of the three complexes with PrP106-126 reflected relatively weak peaks, indicating that their binding affinity was not stronger compared with $[(DMSO)_2H][trans\text{-}Ru(DMSO)_2Cl_4]$. Interestingly, the three complexes displayed intensive inhibitory effect on the aggregation property of the peptide in the TEM and AFM assays. Hence, no direct relationship exists between binding affinity and inhibitory ability.

The oligomers formed by PrP106-126 are stacked by the interface of hydrophobic C-terminal residues 113–126, which may increase the rate of fibril growth [9,19]. The difference between binding affinity and inhibitory effect may also arise from non-bonded interactions including hydrophobic, electrostatic, and π–π interaction, aside from the molecular configuration contribution [52]. Using NAMI-A as an example, the MS data indicated that the complex bound to the peptide in the form of $[Ru(DMSO)(Im)Cl_4]$, which denoted no remaining free metal binding site for the complex to bind with PrP106-126, which was indicated by NMR as well. The hydrophobic interaction between NAMI-A and PrP106-126 interfered with the interface between PrP106-126 molecules, inhibiting the aggregation of the peptide. Therefore, the disaggregation of PrP106-126 does not necessarily rely on metal coordination, specifically, if intense non-bonded interaction can be built between the neuropeptide and the metal complexes.

In summary, the study on the interaction of Ru complexes with PrP106-126 indicated that Ru complexes can bind to PrP106-126 in different binding modes, either through metal coordination or through non-bonded interactions. The complexes with different molecular configurations inhibited the aggregation of PrP106-126 at different degrees. Moreover, aromatic ring-containing Ru complexes showed better inhibitory effects. In addition, the binding affinity does not determine the inhibitory ability of Ru complexes. Ru complexes are compounds that have relatively low cellular toxicity compared with platinum, palladium, and gold complexes. Thus, our study paves the way for effective pharmaceutical products against prion diseases, and further investigation should be carried out to discover potential metallodrugs based on ruthenium complexes.

Abbreviations

PrP^C	Cellular isoform of prion protein
PrP^{Sc}	Abnormal disease-causing isoform of prion protein
PrP106-126	Prion peptide 106-KTNMKHMAGAAAAGAVVGGLG-126
Aβ	Amyloid beta protein
TOCSY	Total correlation spectroscopy
NAMI-A	$[Trans\text{-}RuCl_4(DMSO)(Im)][ImH]$
ThT	Thioflavin-T

Acknowledgments

This work was supported by the National Natural Science Foundation of China (No. 21271185), the National Basic Research Program (No. 2011CB808503), and the Open Fund of State Key Laboratory of Chemical Resource Engineering of Beijing University of Chemical Technology (CRF-2012-C-102).

Appendix A. Supplementary data

Supplementary data to this article can be found online at http://dx.doi.org/10.1016/j.jinorgbio.2013.07.009.

References

[1] S.B. Prusiner, Science 278 (1997) 245–251.
[2] S.B. Prusiner, Proc. Natl. Acad. Sci. U. S. A. 95 (1998) 13363–13383.
[3] C. Korth, B. Stierli, P. Streit, M. Moser, O. Schaller, R. Fischer, W. Schulz-Schaeffer, H. Kretzschmar, A. Raeber, U. Braun, F. Ehrensperger, S. Hornemann, R. Glockshuber, R. Riek, M. Billeter, K. Wuthrich, B. Oesch, Nature 390 (1997) 74–77.
[4] J.F. Diedrich, P.E. Bendheim, Y.S. Kim, R.I. Carp, A.T. Haase, Proc. Natl. Acad. Sci. U. S. A. 88 (1991) 375–379.
[5] M.F. Jobling, X. Huang, L.R. Stewart, K.J. Barnham, C. Curtain, I. Volitakis, M. Perugini, A.R. White, R.A. Cherny, C.L. Masters, C.J. Barrow, S.J. Collins, A.I. Bush, R. Cappai, Biochemistry 40 (2001) 8073–8084.
[6] E. Gaggelli, F. Bernardi, E. Molteni, R. Pogni, D. Valensin, G. Valensin, M. Remelli, M. Luczkowski, H. Kozlowski, J. Am. Chem. Soc. 127 (2004) 996–1006.
[7] H.Z. Soprana, L.C. Souza, V. Debbas, F.R.M. Laurindo, Exp. Toxicol. Pathol. 63 (2011) 229–236.
[8] P. Stańczak, H. Kozłowski, Biochem. Biophys. Res. Commun. 352 (2007) 198–202.
[9] K.M. Pan, M. Baldwin, J. Nguyen, M. Gasset, A. Serban, D. Groth, I. Mehlhorn, Z. Huang, R.J. Fletterick, F.E. Cohen, Proc. Natl. Acad. Sci. U. S. A. 90 (1993) 10962–10966.
[10] M.F. Jobling, L.R. Stewart, A.R. White, C. McLean, A. Friedhuber, F. Maher, K. Beyreuther, C.L. Masters, C.J. Barrow, S.J. Collins, R. Cappai, J. Neurochem. 73 (1999) 1557–1565.
[11] F. Tagliavini, F. Prelli, L. Verga, G. Giaccone, R. Sarma, P. Gorevic, B. Ghetti, F. Passerini, E. Ghibaudi, G. Forloni, Proc. Natl. Acad. Sci. U. S. A. 90 (1993) 9678–9682.
[12] D.R. Brown, B. Schmidt, H.A. Kretzschmar, Nature 380 (1996) 345–347.
[13] J. Chabry, C. Ratsimanohatra, I. Sponne, P.P. Elena, J.P. Vincent, T. Pillot, J. Neurosci. 23 (2003) 462–469.
[14] D.R. Brown, Biochem. J. 352 (2000) 511–518.
[15] A. Corsaro, S. Thellung, V. Villa, M. Nizzari, T. Florio, Int. J. Mol. Sci. 13 (2012) 8648–8669.
[16] D.L. Rymer, T.A. Good, J. Neurochem. 75 (2000) 2536–2545.
[17] C. Selvaggini, L. Degioia, L. Cantu, E. Ghibaudi, L. Diomede, F. Passerini, G. Forloni, O. Bugiani, F. Tagliavini, M. Salmona, Biochem. Biophys. Res. Commun. 194 (1993) 1380–1386.
[18] F. Chiti, C.M. Dobson, Annu. Rev. Biochem. 75 (2006) 333–366.
[19] M. Grabenauer, C. Wu, P. Soto, J.E. Shea, M.T. Bowers, J. Am. Chem. Soc. 132 (2009) 532–539.
[20] P. Walsh, P. Neudecker, S. Sharpe, J. Am. Chem. Soc. 132 (2010) 7684–7695.
[21] R. Liu, R. Su, M. Liang, R. Huang, M. Wang, W. Qi, Z. He, Curr. Med. Chem. 19 (2012) 4157–4174.
[22] Y. Liu, Y. Han, J. Song, Y. Wang, Y. Jing, Q. Shi, C. Tian, Z. Wang, C. Li, J. Han, X. Dong, Int. J. Biochem. Cell Biol. 43 (2011) 768–774.
[23] I. Turi, C. Kállay, D. Szikszai, G. Pappalardo, G. Di Natale, P. De Bona, E. Rizzarelli, I. Sóvágó, J. Inorg. Biochem. 104 (2010) 885–891.
[24] K.J. Barnham, V.B. Kenche, G.D. Ciccotosto, D.P. Smith, D.J. Tew, X. Liu, K. Perez, G.A. Cranston, T.J. Johanssen, I. Volitakis, A.I. Bush, C.L. Masters, A.R. White, J.P. Smith, R.A. Cherny, R. Cappai, Proc. Natl. Acad. Sci. U. S. A. 105 (2008) 6813–6818.
[25] M.P. Cuajungco, C.J. Frederickson, A.I. Bush, Subcell. Biochem. 38 (2005) 235–254.
[26] T. Storr, M. Merkel, G.X. Song-Zhao, L.E. Scott, D.E. Green, M.L. Bowen, K.H. Thompson, B.O. Patrick, H.J. Schugar, C. Orvig, J. Am. Chem. Soc. 129 (2007) 7453–7463.
[27] Y. Wang, J. Xu, L. Wang, B. Zhang, W. Du, Chem. Eur. J. 16 (2010) 13339–13342.
[28] Y. Wang, L. Feng, B. Zhang, X. Wang, C. Huang, Y. Li, W. Du, Inorg. Chem. 50 (2011) 4340–4348.
[29] M.J. Clarke, Coord. Chem. Rev. 236 (2003) 209–233.
[30] C.G. Hartinger, M.A. Jakupec, S. Zorbas-Seifried, M. Groessl, A. Egger, W. Berger, H. Zorbas, P.J. Dyson, B.K. Keppler, Chem. Biodivers. 5 (2008) 2140–2155.
[31] M.J. Clarke, F. Zhu, D.R. Frasca, Chem. Rev. 99 (1999) 2511–2533.
[32] H. Chen, J.A. Parkinson, S. Parsons, R.A. Coxall, R.O. Gould, P.J. Sadler, J. Am. Chem. Soc. 124 (2002) 3064–3082.
[33] D. Valensin, P. Anzini, E. Gaggelli, N. Gaggelli, G. Tamasi, R. Cini, C. Gabbiani, E. Michelucci, L. Messori, H. Kozlowski, G. Valensin, Inorg. Chem. 49 (2010) 4720–4722.
[34] N.P. Cook, V. Torres, D. Jain, A.A. Marti, J. Am. Chem. Soc. 133 (2011) 11121–11123.
[35] I.P. Evans, A. Spencer, G. Wilkinson, J. Chem. Soc. Dalton Trans. (1973) 204–209.
[36] B.R. James, E. Ochiai, G.L. Rempel, Inorg. Nucl. Chem. Lett. 7 (1971) 781–784.
[37] E. Alessio, G. Mestroni, G. Nardin, W.M. Attia, M. Calligaris, G. Sava, S. Zorzet, Inorg. Chem. 27 (1988) 4099–4106.
[38] E. Alessio, G. Balducci, M. Calligaris, G. Costa, W.M. Attia, G. Mestroni, Inorg. Chem. 30 (1991) 609–618.
[39] G. Mestroni, E. Alessio, G. Sava, WO Patent, WO/1998/000, 4311998.
[40] F.P. Dwyer, H.A. Goodwin, E.C. Gyarfas, Aust. J. Chem. 16 (1962) 42–50.
[41] B.P. Sullivan, D.J. Salmon, T.J. Meyer, Inorg. Chem. 17 (1978) 3334–3341.
[42] M.I. Webb, R.A. Chard, Y.M. Al-Jobory, M.R. Jones, E.W.Y. Wong, C.J. Walsby, Inorg. Chem. 51 (2011) 954–966.
[43] M.I. Webb, C.J. Walsby, Dalton Trans. 40 (2011) 1322–1331.
[44] I. Kostova, Curr. Med. Chem. 13 (2006) 1085–1107.

[45] S.R. Byeon, J.H. Lee, J.H. Sohn, D.C. Kim, K.J. Shin, K.H. Yoo, I.M. Jung, W.K. Lee, D.J. Kim, Bioorg. Med. Chem. Lett. 17 (2007) 1466–1470.
[46] J.H. Byun, H.Y. Kima, Y.S. Kima, I.M. Jung, D.J. Kim, W.K. Lee, K.H. Yoo, Bioorg. Med. Chem. Lett. 18 (2008) 5591–5593.
[47] V.P.S. Chauhan, I. Ray, A. Chauhan, J. Wegiel, H.M. Wisniewski, Neurol. Res. 7 (1997) 805–809.
[48] B.J. Blanchard, A. Chen, L.M. Rozeboom, K.A. Stafford, P. Weigele, V.M. Ingram, Proc. Natl. Acad. Sci. U. S. A. 101 (2004) 14326–14332.
[49] B.A. Chromy, R.J. Nowak, M.P. Lambert, K.L. Viola, L. Chang, P.T. Velasco, B.W. Jones, S.J. Fernandez, P.N. Lacor, P. Horowitz, C.E. Finch, G.A. Krafft, W.L. Klein, Biochemistry 42 (2003) 12749–12760.
[50] M. Arimon, I. Díez-Pérez, M.J. Kogan, N. Durany, E. Giralt, F. Sanz, X. Fernàndez-Busquets, FASEB J. 19 (2005) 1344–1346.
[51] J. Laurén, D.A. Gimbel, H.B. Nygaard, J.W. Gilbert, S.M. Strittmatter, Nature 457 (2009) 1128–1132.
[52] G. Ma, F. Huang, X. Pu, L. Jia, T. Jiang, L. Li, Y. Liu, Chem. Eur. J. 17 (2011) 11657–11666.